Published in final edited form as:
Biomed Microdevices. 2014 February ; 16(1): 97–106. doi:10.1007/s10544-013-9809-1.

System architecture for a magnetically guided endovascular microcatheter

Ryan S. Sincic, R.S.S[1], **Curtis J. Caton, C.J.C.**[2], **Prasheel Lillaney, P.L.**[1], **Scott Goodfriend, S.G.**[2], **Jason Niemi, J.N.**[2], **Alastair J. Martin, A.J.M.**[1], **Aaron D. Losey, A.D.L.**[1], **Neel Shah, N.S.**[1], **Erin J. Yee, E.J.Y.**[1], **Lee Evans, L.E.**[1], **Vincent Malba, V.M.**[1], **Anthony F. Bernhardt, A.F.B.**[1], **Fabio Settecase, F.S.**[1], **Daniel L. Cooke, D.L.C.**[1], **Maythem Saeed, M.S.**[1], **Mark W. Wilson, M.W.W.**[1], and **Steven W. Hetts, S.W.H.**[1]

[1]Department of Radiology and Biomedical Imaging, University of California San Francisco, San Francisco CA

[2]Department of Bioengineering and Therapeutic Sciences, University of California San Francisco, San Francisco CA

Abstract

Magnetic resonance imaging (MRI) guided minimally invasive interventions are an emerging technology. We developed a microcatheter that utilizes micro-electromagnets manufactured on the distal tip, in combination with the magnetic field of a MRI scanner, to perform microcatheter steering during endovascular surgery. The aim of this study was to evaluate a user control system

Corresponding author Steven W. Hetts, MD 185 Berry Street, Suite 350, San Francisco, CA 94107 Department of Radiology and Biomedical Imaging University of California, San Francisco Phone: (415) 206-6607 Fax: (415) 206-4004 Steven.Hetts@ucsf.edu.
Ryan S. Sincic, MS 1001 Potrero Avenue, Room 1X57, San Francisco, CA 94110 Department of Radiology and Biomedical Imaging University of California, San Francisco San Francisco, USA
Curtis J Caton, MS 1700 4th Street Byers Hall Room 216, San Francisco, CA 94143 Department of Bioengineering and Therapeutic Sciences University of California San Francisco San Francisco, USA
Prasheel Lillaney, PhD 185 Berry Street, Suite 350, San Francisco, CA 94107 Department of Radiology and Biomedical Imaging University of California, San Francisco San Francisco, USA
Scott Goodfriend, MS 1700 4th Street Byers Hall Room 216, San Francisco, CA 94143 Department of Bioengineering and Therapeutic Sciences University of California San Francisco San Francisco, USA
Jason Niemi, MS 1700 4th Street Byers Hall Room 216, San Francisco, CA 94143 Department of Bioengineering and Therapeutic Sciences University of California San Francisco San Francisco, USA
Alastair J. Martin, PhD 505 Parnassus Ave., Suite L-310, San Francisco, CA 94131 Department of Radiology and Biomedical Imaging University of California, San Francisco San Francisco, USA
Aaron D. Losey, MS 185 Berry Street, Suite 350, San Francisco, CA 94107 Department of Radiology and Biomedical Imaging University of California, San Francisco San Francisco, USA
Neel Shah, MS 185 Berry Street, Suite 350, San Francisco, CA 94107 Department of Radiology and Biomedical Imaging University of California, San Francisco San Francisco, USA
Erin J. Yee, BS 185 Berry Street, Suite 350, San Francisco, CA 94107 Department of Radiology and Biomedical Imaging University of California, San Francisco San Francisco, USA
Lee Evans, BS 185 Berry Street, Suite 350, San Francisco, CA 94107 Department of Radiology and Biomedical Imaging University of California, San Francisco San Francisco, USA
Vincent Malba, PhD 185 Berry Street, Suite 350, San Francisco, CA 94107 Department of Radiology and Biomedical Imaging University of California, San Francisco San Francisco, USA
Anthony F. Bernhardt, PhD 185 Berry Street, Suite 350, San Francisco, CA 94107 Department of Radiology and Biomedical Imaging University of California, San Francisco San Francisco, USA
Fabio Settecase, MD 185 Berry Street, Suite 350, San Francisco, CA 94107 Department of Radiology and Biomedical Imaging University of California, San Francisco San Francisco, USA
Daniel L. Cooke, MD 185 Berry Street, Suite 350, San Francisco, CA 94107 Department of Radiology and Biomedical Imaging University of California, San Francisco San Francisco, USA
Maythem Saeed, PhD, DVM 185 Berry Street, Suite 350, San Francisco, CA 94107 Department of Radiology and Biomedical Imaging University of California, San Francisco San Francisco, USA
Mark W. Wilson, MD 1001 Potrero Avenue, Room 1X57, San Francisco, CA 94110 Department of Radiology and Biomedical Imaging University of California, San Francisco San Francisco, USA
Steven W. Hetts, MD 185 Berry Street, Suite 350, San Francisco, CA 94107 Department of Radiology and Biomedical Imaging University of California, San Francisco San Francisco, USA

for operating, steering and monitoring this magnetically guided microcatheter. The magnetically-assisted remote control (MARC) microcatheter was magnetically steered within a phantom in the bore of a 1.5 Tesla MRI scanner. Controls mounted in an interventional MRI suite, along with a graphical user interface at the MRI console, were developed with communication enabled via MRI compatible hardware modules. Microcatheter tip deflection measurements were performed by evaluating MRI steady-state free precession (SSFP) images and compared to models derived from magnetic moment interactions and composite beam mechanics. The magnitude and direction of microcatheter deflections were controlled with user hand, foot, and software controls. Data from two different techniques for measuring the microcatheter tip location within a 1.5 Tesla MRI scanner showed correlation of magnetic deflections to our model (R^2: 0.88) with a region of linear response (R^2: 0.98). Image processing tools were successful in autolocating the in vivo microcatheter tip within MRI SSFP images. Our system showed good correlation to response curves and introduced low amounts of MRI noise artifact. The center of the artifact created by the energized microcatheter solenoid was a reliable marker for determining the degree of microcatheter deflection and auto-locating the in vivo microcatheter tip.

Keywords

interventional MRI; microcatheter; endovascular; angiography

1 Introduction

Endovascular interventional procedures are typically performed using x-ray fluoroscopy to track catheters that are manually manipulated by torqueing their extracorporeal (proximal) end in an attempt to steer the intracorporeal (distal) tip through tortuous blood vessels. When a catheter makes several turns through the blood vessel's course it becomes increasingly difficult to mechanically steer the catheter tip by twisting the extracorporeal end. This problem can often be addressed with metallic guide-wires and with catheter designs that incorporate metallic braiding in the catheter walls. Our group designed a microcatheter that utilizes electromagnets manufactured on the distal tip, in combination with the strong main magnetic field of a clinical MRI scanner, to perform microcatheter steering during endovascular interventions (Roberts et al., 2002).

The purpose of this paper is to evaluate the hardware, software and user control systems developed to interface with a MARC microcatheter for endovascular interventions under MRI guidance. Systems were designed to monitor the electrical, magnetic, mechanical, and thermal states of the microcatheter, allowing feedback mechanisms to ensure the safety and quality of device operation. Our steering system for electromagnetic microcatheter navigation involves delivering direct electrical current to the MARC microcatheter electromagnetic coils to create magnetic moments (Roberts et al., 2002; Settecase et al., 2007). Interaction between magnetic dipoles from the MRI main magnetic field (B_0) and the micro-electromagnet manufactured on the MARC microcatheter tip is shown in Fig. 1. This mechanism provided controlled angular deflection of the distal microcatheter tip while an operator pushed or pulled the extra-corporeal end to control advancement and retraction. The previous electromagnet current controller used in steering and microcatheter-heating experiments (Bernhardt et al., 2011; Settecase et al., 2011), included a power source with rheostat knobs to control DC current supplied to each of the orthogonal microcatheter electromagnets.

A variety of technologies exist for automated navigation and steering of angiography catheters, and each system is paired with unique manual and computerized controls (Muller et al., 2012). A mechanical catheter steering system, which uses wires running parallel to the

catheter axis to pull tension on the distal tip, and bend the catheters shape, has been used to link the hand control to catheter deflection (Bowden, 1999; Knight et al., 2008; Oh S, 2005), using buttons, dials and joysticks to control mechanical catheter steering (Gang et al., 2011; Oh S, 2005; Saliba et al., 2006). Alternative approaches have been pursued for magnetic catheter steering, such as the Stereotaxis system, which utilizes variable external magnets to navigate a magnetically-tipped catheter (Ernst et al., 2004; Grady et al., 2000); integrating imaging data to guide catheter motion along a road map, however the Stereotaxis system cannot navigate catheters under real-time MRI guidance, as it is not compatible for use within an MRI scanner, due to its reliance on large permanent magnets. The MARC microcatheter has been designed to be fully compatible for use while scanning with MRI, allowing for simultaneous imaging of 2-D planes or 3-D volumes.

2 Materials and Methods

We set out to develop an automation system for the MARC microcatheter with the following design requirements: (1) deliver user defined levels of current to microcatheter electromagnet lead wires, allowing the user to dictate the direction and amplitude of magnetically induced microcatheter deflection, (2) provide a system that is compatible within an MRI suite, such that peripheral controls can be accessed while performing *in vivo* interventions under MRI guidance, (3) provide data recording interface for the MARC microcatheter's probes, and (4) design a GUI for monitoring and controlling the MARC microcatheter from the MRI console or from hand and foot controls within interventional MRI suite.

The microcatheter magnetic tip (Fig. 1) was manufactured onto the end of the commercially available Cordis Rapid Transit 150cm stainless steel braided microcatheter (Cordis Neurovascular, Inc, Miami Fl), as previously described. The 0.001 inch Copper solenoid windings were wound around a 1.25 mm alumina tube which was subsequently placed over the end of the Cordis Rapid Transit microcatheter. The 0.005 inch copper wire leads were pulled through the microcatheter's inner lumen and the outer surface was then covered with heat shrink.

Development of our control system was accomplished using the following steps: i) modeling microcatheter deflection with magnetic forces, ii) development of system hardware and integration of user interfaces, iii) development of system software. The system was evaluated by testing of current source and measurement variance, testing the system in MRI suite and correlating the test results with models of magnetic deflection.

2.1 Modeling magnetic deflection

The theoretical behavior of magnetic microcatheter deflections can be derived from a beam approximation model. Previously, Settecase et al. (Settecase et al., 2007) modeled the microcatheter as a cantilever beam where the torque produced by the magnetic moment τ_{mag} balances against the torque of the beam attempting to return to the initial state τ_{mech}. Modeling the microcatheter as a hollow cylinder that exits a sheath at its proximal end, and is free to rotate, where forces other than generated magnetic torque are assumed to be negligible, the equation describing the equilibrium, for small deflections, becomes:

$$\tau_{mag} = \tau_{mech}$$
$$\tau_{mag} = m\, B_0 \sin(\gamma - \theta)$$
$$\tau_{mech} = \frac{E\, I_A}{L}\theta$$

where B_0 is the strength of the magnetic field of the MRI scanner, I is the solenoid current, m is the magnetic moment of the solenoid, γ is the initial angle of the microcatheter with respect to the B_0-field, θ is the angle of deflection from the initial angle, E is the elastic modulus of the microcatheter and I_A is the area moment of inertia the microcatheter. As an approximation for endovascular studies, the microcatheter would be considered to have a portion restrained by the vessel wall, and a portion at the distal end of the tip of length L, which in this model is approximated to be free to move without opposing force. This equation can be represented in the following linear form (equation 1):

$$\frac{\theta}{\sin\ (\gamma-\theta)}=\frac{nIABL}{EI_{A}}$$

Using equation 1, microcatheter deflection angles θ can be predicted as a function of applied current and initial orientation within the magnetic field. Where n is the number of turns in the solenoid microcoil, A is the transactional area of the microcatheter. The microcatheter deflection angle θ and associated displacement vector are always in the same plane created by the vectors m and B_0. Fig. 2 shows this characteristic surface for a predefined B_0-field, number of solenoid turns, elastic modulus, and unrestrained microcatheter length.

Previously, the Young's modulus of the MARC microcatheter was determined by physical measurements with axial tensile load deformation testing (Settecase et al., 2007). In the current study we modeled the predicted Young's Modulus with composite beam theory. For this purpose, the MARC microcatheter can be modeled as a simple hollow tube or the composite beam of a hollow-tube with copper wires within the microcatheter lumen; assuming that the wires lie on the bending axis of the microcatheter and when an equal bending moment is applied the wires and microcatheter deflect at the same degree. Using composite beam theory the microcatheter elastic modulus (E_{eqiov}) was calculated as follows:

$$E_{equiv}=E_{cath}+\frac{E_{wire}I_{wire}}{I_{cath}}$$

Where E_{equiv} is the equivalent composite elastic modulus, E_{cath} and E_{wire} are the elastic moduli of the simple hollow-tube microcatheter and wires, and I_{cath} and I_{wire} are the area moment of inertias of the microcatheter and wires. The microcatheter prototypes manufactured by our group have an outer and inner diameter of 0.720 mm and 0.392 mm respectively, and an elastic modulus of 9.46 MPa, as measured without wires within the microcatheter lumen (Settecase et al., 2007). With the addition of four 0.089 mm copper wires in the lumen, the equivalent elastic modulus (E_{eqiov}) is calculated to be 118.7 MPa.

2.2 Design of user control interface

A schematic block diagram outlining the microcatheter control system is shown in Fig. 3. A Microsoft Windows operated computer (PC) accepts input from the user via the GUI at the console as well as remote hand and foot controllers mounted in the interventional MRI suite. The hand controllers tested included commercially available 2-axis (APEM, Haverhill, MA) and 3-axis (IPD Launch, CH Products, Vista, CA) USB joysticks. A row of mounted foot switches (Aquiline, Linemaster Switch Corporation, Woodstock, CT), allow the operator free use of their hands while deflecting the microcatheter via foot controls.

2.3 Design of system hardware

We developed custom hardware modules for the analog to digital (ADC) interface within the MRI scanner suite, including a current controller and voltage measurement circuits. This was designed on the basis that analog signal losses and noise would be more easily compensated for by placing the analog to digital converter as close as possible to the MARC microcatheter, so that only digital signals would be sent over the long lengths of wire (10-20 feet) necessary for communication with the PC which sits in the MRI control room outside the MRI RF isolation room and the region of high magnetic field strength. Two hardware configurations were tested for digital communication between the PC and custom hardware control module (Fig. 3). In the first, a data acquisition unit (NI-DAQ USB-6008; National Instruments, Austin, TX), was connected to the PC via USB, and communicated with hand and foot controllers, using as series of analog and digital I/O ports. Bidirectional data between a custom hardware module and the NI-DAQ was serially transferred over 14 digital I/O lines at 1 MHz. Digital commands sent to the custom module include the amount and polarity of current to deliver. Data returned to the NI-DAQ include thermocouple data and electromagnetic coil lead wire voltage. A second digital communication hardware configuration was developed for interface between the PC and the custom hardware controller, in which a USB microcontroller was added to the custom hardware controller so that digital communication could occur directly between the PC, the current source and analog measurement hardware, without the use of an intermediary digital I/O control board.

2.4 Design of system software

The software design requirements include the ability to parse each of the hardware control sets (joysticks, foot pedals, keyboard) for inputs, use algorithms to translate the hardware control inputs to desired current outputs, digitally communicate with the custom PCB module to output desired current values and record real-time device state data (temperature and voltage data), incorporate appropriate feed-back timing for automatic shutoff protocols when sensing unsafe device states, i.e. above safe operational levels of temperature, voltage, or current.

The system is programmed with LabVIEW software and virtual instrument (VI) code (National Instruments Inc., Austix, TX) run on the PC, with MatLab (MathWorks Inc., Natick, MA) M-script embedded, so LabView is the master program in this software hierarchy and controls when M-script is called. This software platform was selected on the basis that it offers tools for software compliance with FDA quality control, and has been used in medical-surgical control systems including laser pulse control for retinal disease treatment (PASCAL system; OptiMedica, Sunnyvale, CA), and an independent MR research spectrometer add-on to clinical MRI systems (InnerVision MRI Ltd, London, UK) (Paley, 2012).

The GUI can be viewed from monitors at the PC console and within the interventional MRI suite (Fig. 4). Through this interface the user can manually control DC current levels delivered to the electromagnets of the microcatheter with a sliding bar controller. Preprogrammed current waveforms can also be delivered to the microcatheter electromagnets. These waveforms may be represented as single shaped pulses (square, exponentially rising waves, etc.), or as a series of waveform pulse data. The GUI also displays measured microcatheter coil voltage, impedance and temperature sensor data. Built into the program are options to save time stamped data to record files. These mechanisms allow easy experimentation with the microcatheter's electromagnetic response to any programmable current waveform, as well as preprogrammed experiments to be automated by the computer with accuracy in timing, amplitude and associated environmental measurements.

2.5 Remote user controls

Remote controls include hand controllers, joysticks, button panels, and foot switches. Joysticks are used to control the amplitude and polarity of microcatheter electromagnet currents, which are proportional to the angle and direction from the neutral position respectively. A three-axis joystick allows for the operator to control three electromagnet coil currents, for 3-dimensional microcatheter steering. As some applications are suited for one and two axes of magnetic steering, joysticks are programmed to operate microcatheters with one and two electromagnets. In order to experiment with a variety of remote user interfaces, we have sourced commercially available control panels and joysticks, as well as designed custom remotes from components.

Hand and foot controls interface with the NI-DAQ or directly with the PC, depending on electrical mechanism (USB, simple switch, etc.). Software feedback determining the time interval between remote user actuation and associated delivery of current waveforms, are estimated to be on the order of tens of milliseconds. This feedback delay becomes insignificant when compared to MRI image refresh rates and user reaction time. However, it would be possible for waveform data to be made available for triggering on the NI-DAQ, thereby bypassing the PC/CPU and reducing this feedback delay to less than a millisecond. We assume that this route of signal bypass would only be necessary if other processes slowed the CPU.

2.6 Experimental methods

Microcatheter deflection experiments were performed with the MARC microcatheter inside a water phantom, using a clinical 1.5 T MR system, (Philips Intera, Best, Netherlands) and utilized body coil RF transmission for all MR studies. MR scanning was performed with SSFP sequences (TR of 3.9, TE of 1.35, 60 degree flip angle).

For measurement of microcatheter deflection angles, a caliper within PixelStick (Venice, CA) image software was used to determine the vector orientations of the microcatheter within obtained images. Angles were measured by establishing the vector from the tip of sheath to the tip of the microcatheter at the baseline and during current induced magnetic deflection. Since during current driven magnetic deflection an MR artifact develops at the microcatheter tip, the location of the microcatheter tip during deflection was established using two different methodologies. In the first the center of the MR artifact visible at the microcatheter tip was established as the microcatheter tip. In the second, a marking was placed on the last visible point of the microcatheter proximal to the artifact.

The protocol AN091424-01, to study magnetic navigation under MRI guidance in an endovascular porcine model was approved by the institutional animal care and use committee on 2/4/2010.

2.7 Statistical methods

Magnetic microcatheter deflection data were compared between our control system current source and commercially available rheostat current source (Lambda Electronics LPD 422A FM, Mellville, New York). Statistical comparisons were also made between MR image microcatheter tip data using linear regression and calculating the least-squares correlation coefficient. Least squares fits to the beam approximation model were performed on the microcatheter deflection data. These fits were performed over the hollow catheter cylinder model and model for composite beams with the addition of copper wire. The corresponding correlation coefficients for each of these fits were then calculated.

3 Results

The device reliably produced currents in the 0-500 mA range for impedances in the range of coil lead impedances of the previously manufactured MARC devices (10-15 Ω). At low MARC coil lead resistance (5 Ω) and inductances ≥ 6.8 μH, currents saturated above 300 mA. At 10-15 Ω and 0-10 μH, +/− 500 mA of current are reliably delivered to the MARC microcatheter with a variance in current delivery of < 2%. At a coil lead resistance > 20 Ω current outputs above 300 mA diverge from the requested current levels, at which point the output voltage reaches its saturation point of 8.0 V. The MARC microcatheter feedback measurement systems were shown to be within the limits of the multimeter accuracy (2%).

MR images of the MARC microcatheter within a water reservoir phantom are shown in Fig. 5. When the microcatheter is connected to the control module a band artifact was observed along the frequency encode axis, representing a distinct band of noise ~64 MHz. When the microcatheter solenoid was energized with current the band artifact disappears and a clover shaped artifact appears at the microcatheter tip. In order to mitigate the frequency band artifact (Fig. 5A), the coil leads were isolated from the remainder of circuit so when no current is delivered, the coil leads are left open and floating. This isolation was achieved by insertion of two solid-state relays, which are closed by a control signal during current delivery to the coil leads. With the new circuit configuration, there was significant reduction in the band frequency artifact and diffuse noise, with a new subtle single line artifact observed (Fig. 5D).

The angle of microcatheter deflection was measured with MR imaging while energizing the microcatheter solenoid (Fig. 6). Deflection data were tested over two different current sourcing devices (the MARC microcatheter control system and rheostat commercial power supply), and deflection angles measured by two techniques (Fig. 6A and 6B). Fig. 6A shows the deflection angles measured using the change in angle from the microcatheter base to the distal edge of the microcatheter, visible in the MRI image, the relationship between the deflection angle and delivered current over this data set is linear for both the MARC microcatheter control system and the commercial rheostat power supply (linear regression fit R^2: 0.99 for rheostat and 0.98 for MARC microcatheter control system). Fig. 6B shows the angle of deflection measured by using the center of microcatheter MRI artifact to track angular orientation, the relationship between current and deflection angle is also shown to be linear using this alternate technique of measurement (linear regression, R^2: 0.99 for rheostat and 0.98 for control system). Both deflection angle measurement techniques demonstrated agreement between the MARC control system and rheostat.

The least squares regression fit of the microcatheter data to the simple hollow tube model (Fig. 7) showed little correlation ($R^2 < 0.01$ both techniques of angular deflection measurement). The least squares regression fit of the microcatheter data to the composite beam model (Fig. 7), using the addition of copper wire, showed a much more predictive model, with similar goodness of fits for the deflection data measured using the visible microcatheter ($R^2 = 0.88$) and the center of the microcatheter artifact ($R^2 = 0.88$). The composite beam model and simple hollow tube model predicted a Young's Modulus of 123 MPa and 9.5 MPa respectively, for a microcatheter of 0.5 mm inner diameter and 0.75 mm outer diameter.

To evaluate the ability to localize the microcatheter tip location *in vivo*, MR images were taken of the MARC microcatheter in a porcine carotid artery (Fig. 8). From these images we were able to auto-locate the artifact created when the microcatheter tip solenoid was energized, by using a sequence of image processing and analysis steps within MatLab, to

mark the virtual center. Our image processing analysis did not reliably locate the last portion of the visible microcatheter tip proximal to the artifact.

For *in vivo* microcatheter navigation purposes, the MARC microcatheter control system was easy to setup, with convenient physical placement of the user control interfaces while the MARC microcatheter was inserted into the common femoral artery of an anesthetized pig and navigated in the abdominal aorta. DAC recordings were observed via the GUI, without any significant additional noise. SSFP MR imaging of the in vivo microcatheter in a 3 T clinical MR scanner (GE 750 AW; Schenectady, NY) did not reveal any significant new artifacts while the electrical hardware was performing DAC recordings from the MARC microcatheter. In vivo steering experiments were limited due differences in imaging protocols between 1.5 T and 3 T scanners, which affected visualization of the microcatheter tip.

4 Discussion

The hardware performance testing data showed low variability of our current source and measurement systems. Our programmable current source was capable of producing DC currents of ± 0.5 amps, which can be updated at rates as high as 83 kHz (a current wave temporal error of 12 μs). This allowed for adequate electromagnetic steering currents, which will typically operate in the 0.1 - 0.3 ampere range, and provided flexibility in alteration of waveform shape. For monitoring current output, our device was designed to sample electromagnetic coil lead voltage with bit error accuracy of 1.2 millivolts, (measured error <10 mV at 0-8 V) and at a max frequency of 200 kHz (sampling time error of 5 microseconds). This sampling provides coil resistance measurement accuracy of 1.1%.

We successfully applied two different techniques for measuring the location of the deflected microcatheter tip. Both techniques of microcatheter tip localization have similar correlation to our model ($R^2 \sim 0.88$). Both of these techniques show a linear relationship between degree of deflection and current delivery for currents less than 500 mA, and a microcatheter with elastic modulus of greater than 94 MPa. The linear relationship between current and magnetic deflection should allow easier prediction of deflection and possibly allow the user to predefine magnitude of deflection rather than current. As modeled, a catheter with a lesser modulus of elasticity would exit the linear region of this relationship at lower applied currents. To allow greater microcatheter deflection per applied current, future catheter designs will address decreasing total catheter elastic modulus through introducing thinner wires, softer catheter materials, and laser lithographed solenoids. Laser lithography fabrication of solenoid tips will allow for more conductive loops per unit length, providing for greater magnetic moments per unit of applied current.

The addition of intraluminal copper wire to the composite beam model correlated more strongly to measured deflection data. This would be as expected with the assumption that the intraluminal wires bend with the microcatheter, rather than sliding along the microcatheter axis or allowing free motion of the microcatheter with respect to the copper wire.

We have undergone several hardware redesigns in order to compensate for conditions unique to the MRI scanner environment. For example, implementation of a USB microcontroller for simplifying digital data flow between the current source and the PC has caused USB faults, with some MRI RF excitation pulses. We have not been able to source commercial USB microcontrollers that are compatible with high energy RF noise. Sourcing parts that are compatible in 1.5 and 3 T magnetic fields has limited some of our options for commercially available remote controllers. In finding safe equipment for this device, any parts with ferromagnetism must have negligible magnetically induced forces when placed in

the bore of the magnet, and be well secured to equipment housing. Furthermore, device induced MRI artifacts have lead to redesigns to eliminate RF noise produced by system hardware. Microcatheter materials for future designs will incorporate polyetheretherketone braiding, rather than nitinol or stainless steel braiding, to avoid RF heating, imaging artifacts, and ferromagnetic forces.

The orientation of the microcatheter coil magnetic moment with respect to the conical angle it creates with the main magnetic field of the MRI bore determines the direction of the torque on the microcatheter tip with positive and negative current, forcing an increase or a decrease in the conical angle. Future designs should allow the user to perform microcatheter steering using left-right and up-down commands, rather than positive and negative current commands, as are presently implemented.

Metallic thermocouples may be subject to RF induced heating in MRI; unfortunately fiber-optic based MRI compatible temperature probes are generally too large to place within endovascular catheters or affix along side endovascular catheters *in vivo* except in the largest of blood vessels. Internal catheter temperature can be monitored continuously throughout operation. The thermocouple voltage can be sampled at 200 kHz (at 5 microsecond intervals), with a voltage bit error of 1.2 millivolts and an interpolated temperature measurement error of less than 0.5 °C. Given that the FDA requires less than 1 °C change in tissue temperature during brain interventions and less than 2 °C change in body interventions, we aim to measure temperature in increments of 10 fold less than the maximum acceptable change (error of less than 0.1 °C).

Currents escaping from an implanted device may pose a greater risk to the pathologic effects of electrical current due to implantation beyond superficial adipose tissue, which is a poor conductor compared to other tissues, such as muscle, bone and blood (Gabriel et al., 2009). Small amounts of electrical energy (< 0.4 V over < 0.5 ms periods) within the heart are known to induce both atrial and ventricular ectopy (Perrins et al., 1981). As a result, RF ablation catheters for cardiac therapies necessitate delivery of specified RF currents, and are engineered with power meters, impedance, and temperature sensors, as well as current limiters and temperature-threshold shutoffs. Our systems current electrical measurement feedback system would allow for software limits to be programmed that would induce cardiac ectopy or tissue injury.

The center of the microcatheter tip artifact is a reliable marker for microcatheter tip location, when compared to using the last portion of the visible microcatheter tip. Given the current microcatheter construction and image processing techniques, the center of the energized microcatheter artifact is the preferred method for localization of the tip *in vivo*, as we have successfully applied image-processing techniques for microcatheter tip auto-locating. We are continuing to develop techniques for active microcatheter tracking with MR imaging (Schalla et al., 2003).

5 Conclusions

We successfully controlled the magnitude and direction of microcatheter deflections with the device hand, foot and software controls. Hardware performance testing showed low variability of our control and measurement systems and a low introduction of MRI noise artifacts. The center of the artifact created by the energized microcatheter solenoid is a reliable marker for determining the degree of microcatheter deflection and software auto-location of the microcatheter tip.

Acknowledgments

none

Sources of financial support: NIH-NIBIB 1R01EB012031 (Hetts, PI), NIH-NHLBI 1RO1HL076486 (Wilson, PI), American Society of Neuroradiology Research and Education Foundation Scholar Award (Hetts), UCSF Department of Radiology and Biomedical Imaging

References

Bernhardt A, Wilson MW, Settecase F, Evans L, Malba V, Martin AJ, Saeed M, Roberts TP, Arenson RL, Hetts SW. Steerable catheter microcoils for interventional MRI reducing resistive heating. Academic radiology. 2011; 18:270–276. [PubMed: 21075017]

Bowden R. Steerable electrode catheter, USA. 1999

Ernst S, Ouyang F, Linder C, Hertting K, Stahl F, Chun J, Hachiya H, Bansch D, Antz M, Kuck KH. Initial experience with remote catheter ablation using a novel magnetic navigation system: magnetic remote catheter ablation. Circulation. 2004; 109:1472–1475. [PubMed: 15023876]

Gabriel C, Peyman A, Grant EH. Electrical conductivity of tissue at frequencies below 1 MHz. Physics in Medicine and Biology. 2009; 54:4863–4878. [PubMed: 19636081]

Gang ES, Nguyen BL, Shachar Y, Farkas L, Marx B, Johnson D, Fishbein MC, Gaudio C, Kim SJ. Dynamically shaped magnetic fields: initial animal validation of a new remote electrophysiology catheter guidance and control system. Circ Arrhythm Electrophysiol. 2011; 4:770–777. [PubMed: 21690463]

Grady MS, Howard MA 3rd, Dacey RG Jr. Blume W, Lawson M, Werp P, Ritter RC. Experimental study of the magnetic stereotaxis system for catheter manipulation within the brain. J Neurosurg. 2000; 93:282–288. [PubMed: 10930015]

Knight B, Ayers GM, Cohen TJ. Robotic positioning of standard electrophysiology catheters: a novel approach to catheter robotics. J Invasive Cardiol. 2008; 20:250–253. [PubMed: 18460712]

Muller L, Saeed M, Wilson MW, Hetts SW. Remote control catheter navigation: options for guidance under MRI. Journal of cardiovascular magnetic resonance : official journal of the Society for Cardiovascular Magnetic Resonance. 2012; 14:33. [PubMed: 22655535]

Oh S,ZY, Mazgalev T, Natale A, Marrouche N. Novel robotic catheter remote control system: safety and accuracy in delivering RF lesions in all 4 cardiac chambers. Heart Rhythm. 2005; 2:S277–S278.

Paley M. Using LabVIEW and PXI to Develop an Integrated MRI System Controller and Multichannel Spectrometer. 2012

Perrins EJ, Sutton R, Kalebic B, Richards LR, Morley C, Terpstra B. Modern atrial and ventricular leads for permanent cardiac pacing. Br Heart J. 1981; 46:196–201. [PubMed: 7272131]

Roberts TP, Hassenzahl WV, Hetts SW, Arenson RL. Remote control of catheter tip deflection: an opportunity for interventional MRI. Magnetic resonance in medicine : official journal of the Society of Magnetic Resonance in Medicine / Society of Magnetic Resonance in Medicine. 2002; 48:1091–1095. [PubMed: 12465124]

Saliba W, Cummings JE, Oh S, Zhang Y, Mazgalev TN, Schweikert RA, Burkhardt JD, Natale A. Novel robotic catheter remote control system: feasibility and safety of transseptal puncture and endocardial catheter navigation. J Cardiovasc Electrophysiol. 2006; 17:1102–1105. [PubMed: 16879628]

Schalla S, Saeed M, Higgins CB, Martin A, Weber O, Moore P. Magnetic resonance--guided cardiac catheterization in a swine model of atrial septal defect. Circulation. 2003; 108:1865–1870. [PubMed: 14517162]

Settecase F, Hetts SW, Martin AJ, Roberts TP, Bernhardt AF, Evans L, Malba V, Saeed M, Arenson RL, Kucharzyk W, Wilson MW. RF Heating of MRI-Assisted Catheter Steering Coils for Interventional MRI. Academic radiology. 2011; 18:277–285. [PubMed: 21075019]

Settecase F, Sussman MS, Wilson MW, Hetts S, Arenson RL, Malba V, Bernhardt AF, Kucharczyk W, Roberts TP. Magnetically-assisted remote control (MARC) steering of endovascular catheters for interventional MRI: a model for deflection and design implications. Med Phys. 2007; 34:3135–3142. [PubMed: 17879774]

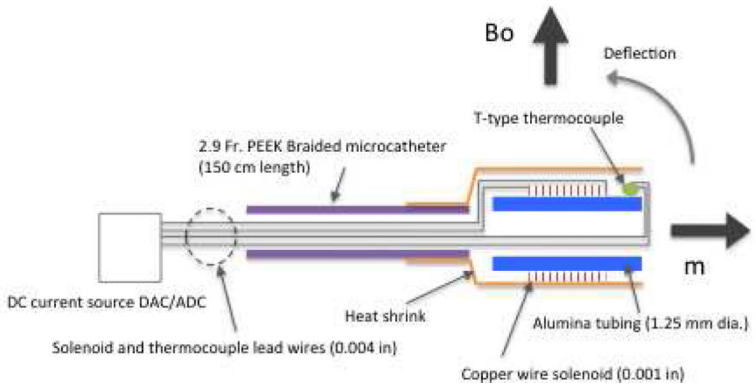

Fig. 1.

MARC microcatheter structure and function. When placed in a magnetic field (Bo) the microcatheter tip deflections can be bi-directionally controlled with the polarity of currents supplied to the solenoid lead wires, which generate magnetic moments (m) at the distal end of the catheter.

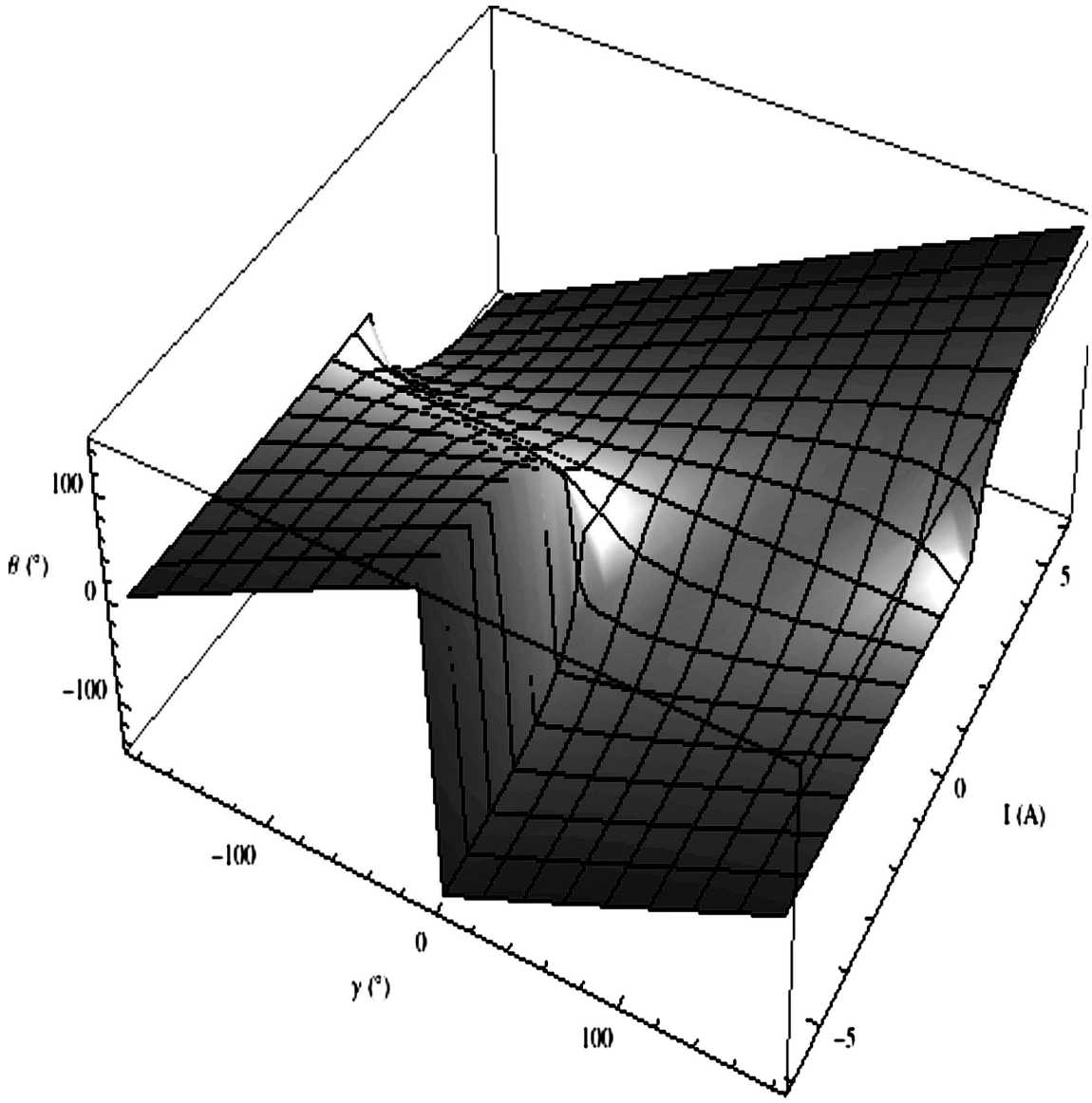

Fig. 2.

Catheter deflection angles plotted as a function of applied current, and initial orientation. Varying the catheter's unrestrained length provides a family of similar surfaces, so that shortening the unrestrained length flattens the characteristic surface and providing more unrestrained catheter length steepens the slope of the response over the domain of this surface.

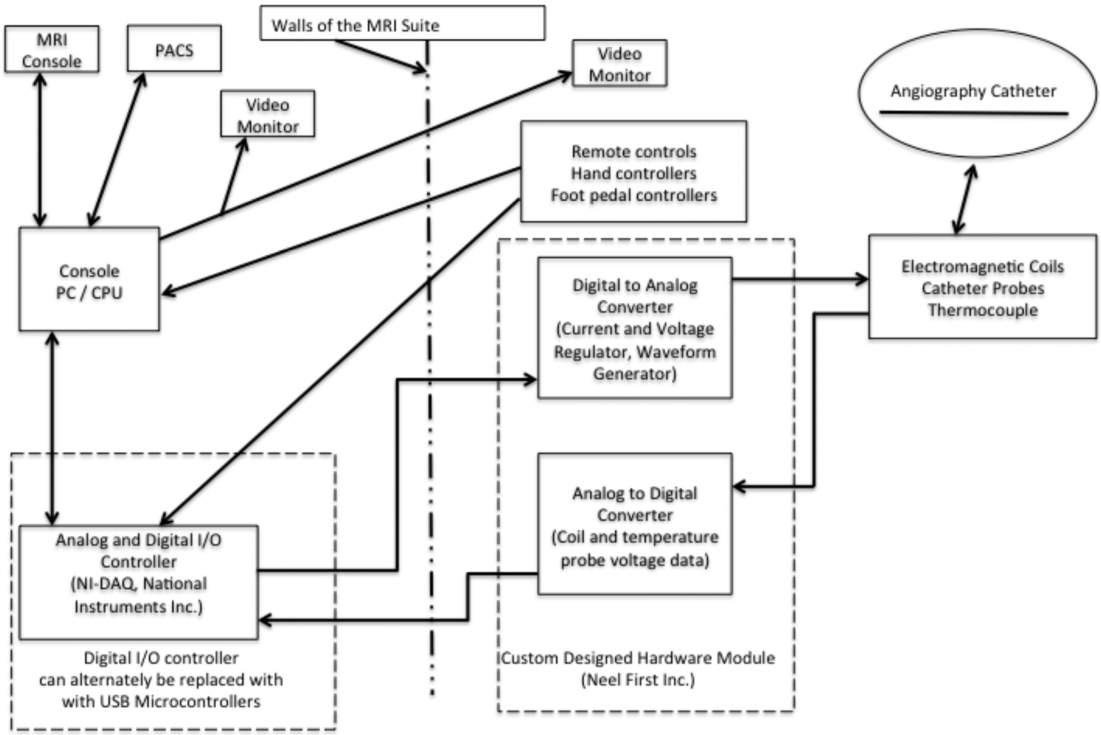

Fig. 3.

Overview of MARC catheter control system hardware configuration. The catheter with electromagnetic tip is represented in the upper right hand corner of the figure. Major components are labeled within boxes and arrows represent data flow. Alternate hardware configurations have been developed, which integrate USB microcontrollers onto the custom hardware PCB module and onto footswitch to relay digital communication via USB to the PC without necessitating the NI-DAQ controller.

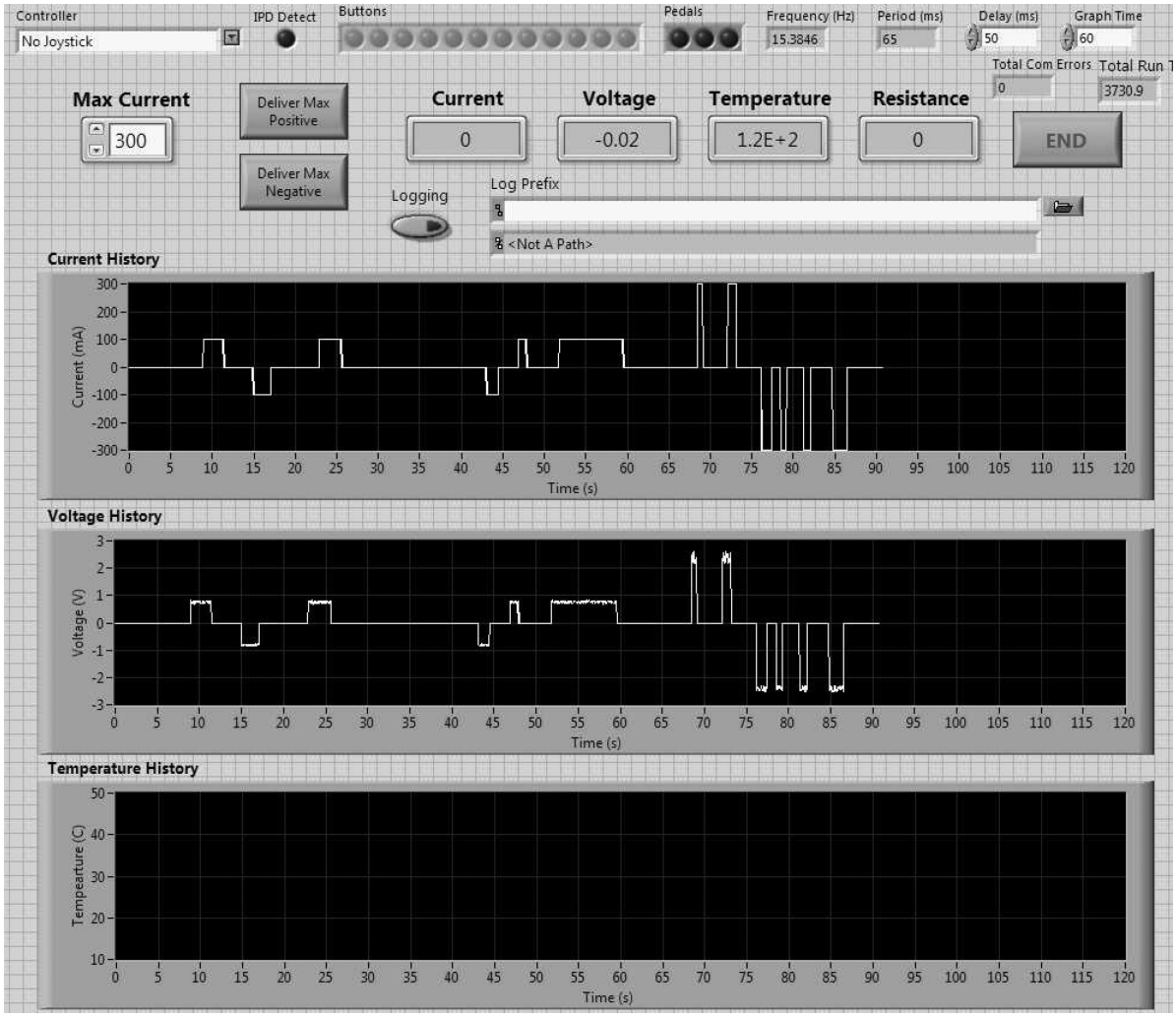

Fig. 4.
Interactive GUI for magnetically guided catheter control system.

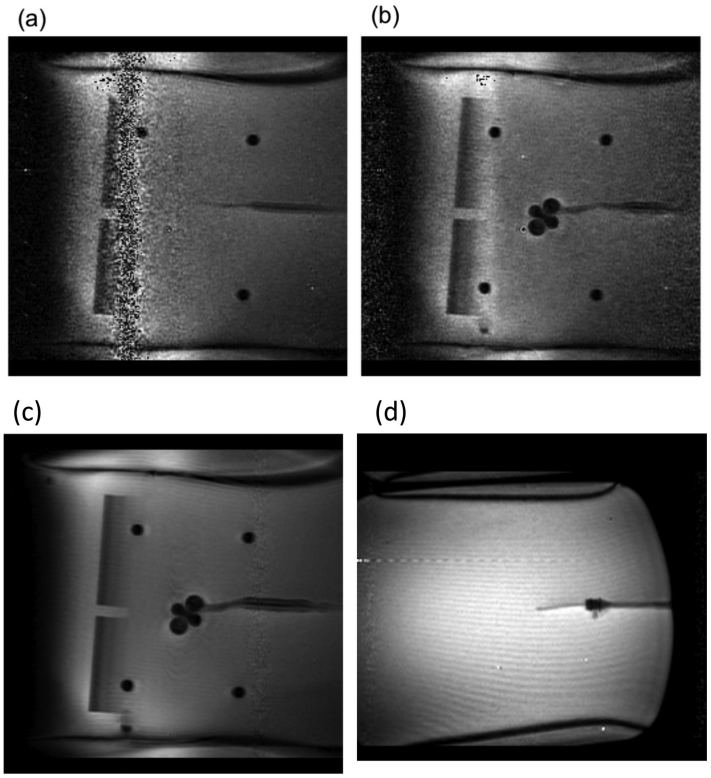

Fig. 5.
MR images of the MARC catheter in a phantom, taken with SSFP sequence with TR of 3.9, TE of 1.35 and 60 degree flip angle. (A) When the catheter is connected to the control module, a band artifact is captured along the frequency encode axis, representing a distinct band of noise ~64 MHz. (B) When the catheter solenoid is energized with current, the band artifact disappears, and a clover shaped artifact appears at the catheter tip. (C) The rheostat power source while energizing the MARC catheter produces less diffuse noise, and a subtle band of frequency related noise. Coils were energized to 300 mA in B and C. (D) The frequency band artifact is significantly reduced after isolation of coil leads. A new subtle single line artifact is observed after cleaning up the band frequency artifact and diffuse noise.

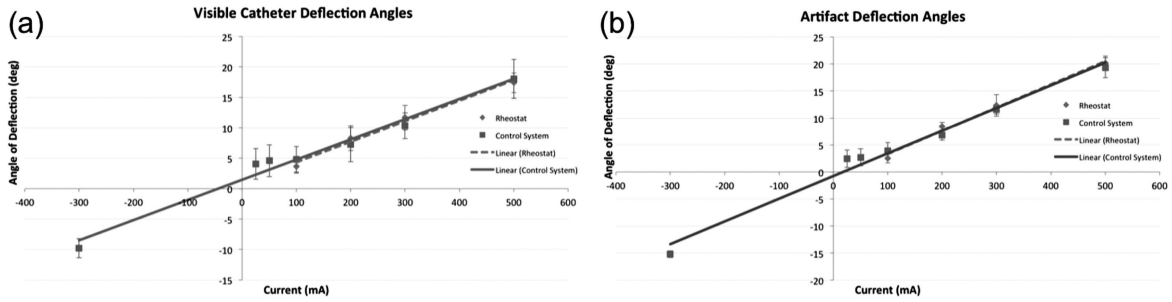

Fig. 6.

Deflection measurements using MR imaging while energizing the catheter solenoid, with two techniques of measuring angular catheter deflection (A-B). (A) Deflection angles measured using most distal visible point of the catheter (linear regression fit with, R^2: 0.99 for rheostat and 0.98 for control system). (B) Angles of deflection measured using the center of catheter MRI artifact (linear regression fit with, R^2: 0.99 for rheostat and 0.98 for control system). The deflection angle data points are presented as means and standard error of the means, calculated from n = 5.

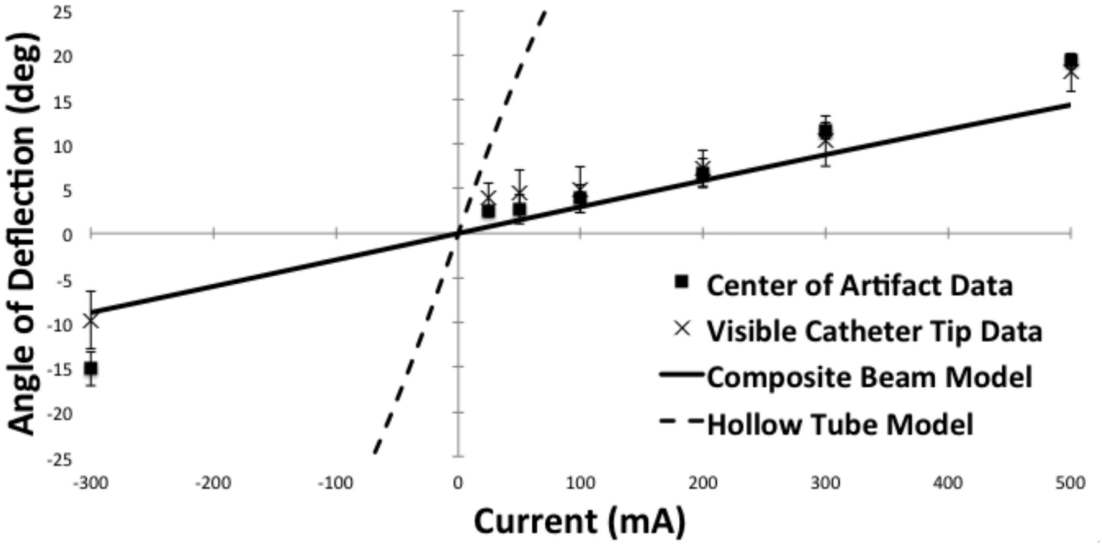

Fig. 7.

Deflection data fit to two different models of catheter mechanical elasticity. The least squares regression fit of the catheter data to the composite beam model, using the addition of copper wire, is shown in the solid line, and correlation with the deflection data measured using the visible catheter tip ($R^2 = 0.88$) and the center of the catheter artifact ($R^2 = 0.88$). The least squares regression fit of the catheter data to a simple hollow tube is shown with the dashed line and has little correlation with measured deflection data ($R^2 < .01$ both techniques of angular deflection measurement).

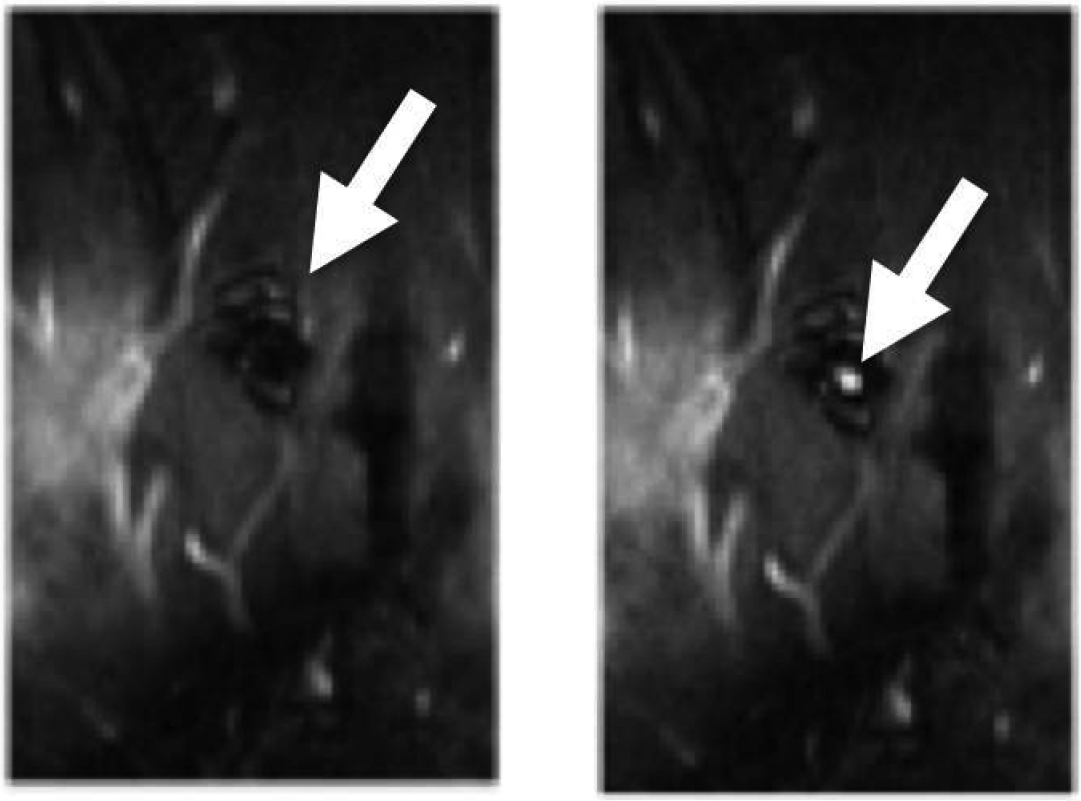

Fig. 8.

1.5 T MRI SSFP images of MARC catheter in vivo within a porcine carotid artery. Artifact created by energizing the catheter is visible (left). The energized catheter tip was auto-located by software using a sequence of image processing and analysis steps to mark the virtual center of the artifact (right).